

Analysis of operator splitting in the non-asymptotic regime for nonlinear reaction-diffusion equations. Application to the dynamics of premixed flames

Stéphane Descombes^{†**} Max Duarte^{†||} Thierry Dumont[‡]
 Frédérique Laurent[§] Violaine Louvet[‡] Marc Massot[§]

April 19, 2022

Abstract

In this paper we mathematically characterize through a Lie formalism the local errors induced by operator splitting when solving nonlinear reaction-diffusion equations, especially in the non-asymptotic regime. The non-asymptotic regime is often attained in practice when the splitting time step is much larger than some of the scales associated with either source terms or the diffusion operator when large gradients are present. In a series of previous works a reduction of the asymptotic orders for a range of large splitting time steps related to very short time scales in the nonlinear source term has been studied, as well as that associated with large gradients but for linearized equations. This study provides a key theoretical step forward since it characterizes the numerical behavior of splitting errors within a more general nonlinear framework, for which new error estimates can be derived by coupling Lie formalism and regularizing effects of the heat equation. The validity of these theoretical results is then assessed in the framework of two numerical applications, a KPP-type reaction wave where the influence of stiffness on local error estimates can be thoroughly investigated; and a much more complex problem, related to premixed flame dynamics in the low Mach number regime with complex chemistry and detailed transport, for which the present theoretical study shows to provide relevant insights.

Keywords

Operator splitting, error bounds, reaction-diffusion, traveling waves, combustion

AMS subject classifications

65M15, 65L04, 65Z05, 35A35, 35K57, 35C07

[†]Univ. Nice Sophia Antipolis, CNRS, LJAD, UMR 7351, 06100 Nice, France.

^{**}INRIA Sophia Antipolis-Méditerranée Research Center, Nachos project-team, 06902 Sophia Antipolis Cedex, France (stephane.descombes@unice.fr).

^{||}CCSE, Lawrence Berkeley National Laboratory, 1 Cyclotron Rd. MS 50A-1148, Berkeley, CA 94720, USA (MDGonzalez@lbl.gov).

[‡]Institut Camille Jordan - UMR CNRS 5208, Université de Lyon, Université Lyon 1, INSA de Lyon 69621, Ecole Centrale de Lyon, 43 Boulevard du 11 novembre 1918, 69622 Villeurbanne Cedex, France (tdumont,louvet@math.univ-lyon1.fr).

[§]Laboratoire EM2C - UPR CNRS 288, Ecole Centrale Paris, Grande Voie des Vignes, 92295 Châtenay-Malabry Cedex, France (frederique.laurent,marc.massot@ecp.fr).

1 Introduction

Operator splitting techniques [40, 32], also called fractional steps methods [41, 42, 44], were introduced with the main objective of saving computational costs. A complex and potentially large problem could be then split into smaller or subproblems of different nature with an important reduction of the algorithmic complexity and computational requirements. The latter characteristics were largely exploited over the past years to carry out numerical simulations in several domains going from biomedical models, to combustion or air pollution modeling applications. Moreover, these methods continue to be widely used mainly because of their simplicity of implementation and their high degree of liberty in terms of choice of dedicated numerical solvers for the split subproblems. They are in particular suitable for stiff problems, for which a special care must be addressed to choose adequate and stable methods that properly handle and damp out fast transients inherent, for instance, to the reaction [43] or diffusion [34] equations. In most applications first and second order splitting schemes are implemented for which a general mathematical background is available (see, *e.g.*, [19] for ODEs and [24] for PDEs). Even though these schemes are usually efficient for the solution of time dependent equations, it is well known that they might suffer from order reduction in the stiff case, and some studies were conducted to explain this phenomenon. Another potential issue is the accuracy loss related to the boundary conditions for PDEs with transport operators, solved in a splitting framework. This problem was investigated, for instance, in [23, 24] for advection-reaction equations and mathematically described in [22] in a more general framework for two linear operators generating strongly continuous semigroups. For stiff applications, several works [2, 45, 39, 35] illustrated perturbing effects on the accuracy of splitting approximations for multi-scale PDEs. Multi-scale features in time are commonly related to physical dynamics characterized by a broad range of time scales, while steep gradients or large higher order spatial derivatives induce similar phenomena in space. In all these cases the standard numerical analysis of splitting errors remains valid for asymptotically small time steps, and rapidly becomes insufficient for stiff problems. A better understanding of splitting methods for such regimes can be thus justified by the fact that practical considerations often suggest the use of relatively large time steps in order to ease heavy computational costs related to the numerical simulation of complex applications.

For PDEs disclosing physical time scales much faster than the splitting time step, a theoretical study was conducted in [38] in the framework of a linear system of ODEs issued from a reaction-diffusion equation with a linear source term and diagonal diffusion. Splitting errors with relatively large splitting time steps were therefore mathematically described, whereas splitting schemes ending with the stiffest operator were also shown to be more accurate. Similar conclusions were drawn in [28] for nonlinear systems of ODEs. A mathematical framework was then introduced in [7] to describe these errors for nonlinear reaction-diffusion equations. This work further analyzed order reduction in direct relation to the nonlinearity of the equations, and in particular confirmed better performances for splitting schemes that finish with the time integration of the stiffest operator. Other theoretical studies were also conducted to investigate splitting errors and in particular to derive alternative estimates exhibiting deviations from classical asymptotic estimates. A numerical analysis based on analytic semi-group theory was first considered in [26] for linear operators, and then in [6] for a system of ODEs issued from a discretized linear reaction-diffusion equation with solutions of high spatial gradients. The latter approach, based on the exact representation of local splitting errors introduced in [8], was then recast in [11] in infinite dimension for a linearized reaction-diffusion equation. Whether the analysis is performed in finite or infinite dimension, the resulting estimates predict an effective order reduction for linear or linearized reaction-diffusion equations. For instance, local errors related to a Lie approximation of first order exhibits deviations from $\mathcal{O}(\Delta t^2)$ observed in the asymptotic regime to $\mathcal{O}(\Delta t^{1.5})$ for a range of relatively large splitting time step Δt [6, 11]. Similarly, Strang error approximations deviate from $\mathcal{O}(\Delta t^3)$ to $\mathcal{O}(\Delta t^2)$ in infinite dimension [11], or from $\mathcal{O}(\Delta t^3)$ in the asymptotic regime to $\mathcal{O}(\Delta t^{2.5})$, and potentially $\mathcal{O}(\Delta t^{1.5})$ in various ranges of splitting time steps for the corresponding semi-discretized problem [6].

All of these studies shed some light on the behavior of splitting methods for stiff PDEs and in

particular for non-arbitrarily small splitting time steps. Nevertheless, a mathematical description in a more general and fully nonlinear framework seems natural to further investigate these schemes. No rigorous analysis of these configurations is however available so far in the literature. The relevance of such a study is hence justified not only because most of physical models disclose important stiffness but because short splitting time steps heavily restrict the efficiency of splitting methods. A better understanding of these schemes for non-asymptotic regimes, that is, for splitting time steps much larger than the fast scales associated with each operator, seems therefore necessary to enhance the numerical performance of such methods.

We conduct in this study the numerical analysis of splitting errors for time dependent PDEs in the case of nonlinear reaction-diffusion equations. The approach adopted is based on previous analyses carried out with linear operators and analytic semi-group theory, as well as the exact representation of splitting errors. The inherent nonlinearity of the equations is handled through the Lie formalism. In this work we limit the study to diagonal diffusion terms as a first step, and we neglect as well the influence of boundary conditions of the PDEs. We derive local error bounds that consistently describe classical orders, as well as a hierarchy of alternative estimates more relevant in non-asymptotic regimes related to various ranges of large splitting time step. In particular for large splitting times and problems modeling steep fronts, such a mathematical characterization shows that this deviation from the asymptotic behavior actually involves smaller numerical errors than the ones expected with the asymptotic classical orders. The resulting theoretical estimates are then evaluated for PDEs modeling traveling waves, for which stiffness can be easily introduced in the equations and thus allows us to systematically investigate various stiff scenarios. To further assess these theoretical findings for more complex and realistic applications, we investigate splitting errors for the simulation of premixed flame dynamics in the low Mach number regime with complex chemistry and detailed transport. We therefore introduce a new splitting method compatible with the low Mach number constraint and show how the theoretical results we have obtained allow us to gain fundamental insight in the analysis of splitting errors, thus paving the way for further theoretical studies as well as new numerical algorithms.

The paper is organized as follows. We carry out the numerical analysis of operator splitting in Section 2, for nonlinear reaction-diffusion equations. We then evaluate in Section 3 the previous theoretical estimates in the context of PDEs modeling traveling waves, in particular with a KPP-type of nonlinearity. A counterflow premixed flame is studied in Section 4, in the low Mach number regime with complex chemistry and detailed transport.

2 Analysis of operator splitting errors in the non-asymptotic regime

In this section we conduct a mathematical description of splitting local errors for nonlinear reaction-diffusion equations. First, we recall some previous theoretical results for operator splitting in a linear framework, and then we investigate the nonlinear case by using Lie derivative calculus.

2.1 Error formulae in the linear framework

Let us consider two general linear operators A and B , for which the exponentials e^{-tA} and e^{-tB} can be understood as a formal series. The first order Lie and the second order Strang splitting formulas to approximate $e^{-t(A+B)}$ are, respectively, given by

$$\mathcal{L}(t) = e^{-tA}e^{-tB}, \quad \mathcal{S}(t) = e^{-tA/2}e^{-tB}e^{-tA/2}. \quad (1)$$

In what follows we will give an exact representation of the difference between $e^{-t(A+B)}$ and its Lie and Strang approximations (1), by recalling some results proved in [6] and [8]. We introduce the

following notations: $\partial_A B$ denotes the commutator between A and B ,

$$\partial_A B = [A, B] = AB - BA, \quad (2)$$

and thus

$$\partial_A^2 B = [A, [A, B]], \quad \partial_B^2 A = [B, [B, A]]. \quad (3)$$

Theorem 1. *The following identities hold*

$$\mathcal{L}(t) = e^{-t(A+B)} + \int_0^t \int_0^s e^{-(t-s)(A+B)} e^{-(s-r)A} (\partial_A B) e^{-rA} e^{-sB} dr ds, \quad (4)$$

$$\begin{aligned} \mathcal{S}(t) &= e^{-t(A+B)} \\ &+ \frac{1}{4} \int_0^t \int_0^s (s-r) e^{-(t-s)(A+B)} e^{-(s-r)A/2} (\partial_A^2 B) e^{-rA/2} e^{-sB} e^{-sA/2} dr ds \\ &- \frac{1}{2} \int_0^t \int_0^s (s-r) e^{-(t-s)(A+B)} e^{-sA/2} e^{-rB} (\partial_B^2 A) e^{-(s-r)B} e^{-sA/2} dr ds. \end{aligned} \quad (5)$$

Formula (4) was originally introduced in [36]. Additionally, we have the following equivalent representations which turn out to be more convenient in the nonlinear case.

Corollary 1. *Considering (4) and (5), the following identities hold*

$$\mathcal{L}(t) = e^{-t(A+B)} + \int_0^t \int_0^s e^{-sA} e^{-rB} (\partial_A B) e^{-(s-r)B} e^{-(t-s)(A+B)} dr ds, \quad (6)$$

$$\begin{aligned} \mathcal{S}(t) &= e^{-t(A+B)} \\ &+ \frac{1}{4} \int_0^t \int_0^s (s-r) e^{-sA/2} e^{-sB} e^{-rA/2} (\partial_A^2 B) e^{-(s-r)A/2} e^{-(t-s)(A+B)} dr ds \\ &- \frac{1}{2} \int_0^t \int_0^s (s-r) e^{-sA/2} e^{-(s-r)B} (\partial_B^2 A) e^{-rB} e^{-sA/2} e^{-(t-s)(A+B)} dr ds. \end{aligned} \quad (7)$$

Proof. It suffices to compute the adjoint of (4) and (5), and noticing that according to the definition of exponentials, we have $(e^{tA})^* = e^{tA^*}$, $(e^{tA} e^{tB})^* = e^{tB^*} e^{tA^*}$, and with (2) and (3): $(\partial_A B)^* = \partial_{B^*} A^*$, $(\partial_A^2 B)^* = \partial_{A^*}^2 B^*$, and $(\partial_B^2 A)^* = \partial_{B^*}^2 A^*$. \square

2.2 Splitting errors for nonlinear reaction-diffusion equations

We consider the scalar reaction-diffusion equation

$$\left. \begin{aligned} \partial_t u - \partial_x^2 u &= f(u), & x \in \mathbb{R}, t > 0, \\ u(x, 0) &= u_0(x), & x \in \mathbb{R}. \end{aligned} \right\} \quad (8)$$

Considering the maximum norm $\|\cdot\|_\infty$, we denote by $C_b(\mathbb{R})$ the space of functions bounded over \mathbb{R} , and by $C_b^\infty(\mathbb{R})$ the functions of class C^∞ bounded over \mathbb{R} . We assume that f is a function of class C^∞ , from \mathbb{R} to itself, such that there exists $R > 0$ for which

$$|r| \geq R \Rightarrow rf(r) \leq 0. \quad (9)$$

Without loss of generality we assume that $f(0) = 0$ and $R = 1$. If u_0 belongs to $C_b^\infty(\mathbb{R})$, it can be then shown that equation (8) has a unique solution [4], and we represent the solution $u(t, \cdot)$ as $T^t u_0$, where T^t is the semi-flow associated with (8). Moreover such a function u is infinitely differentiable over $\mathbb{R} \times (0, \infty)$, and the following estimate holds [4],

$$\|T^t u_0\|_\infty \leq \max(\|u_0\|_\infty, 1). \quad (10)$$

Given v_0 and w_0 in $C_b^\infty(\mathbb{R})$, we consider the following equations:

$$\left. \begin{aligned} \partial_t v - \partial_x^2 v &= 0, & x \in \mathbb{R}, t > 0, \\ v(x, 0) &= v_0(x), & x \in \mathbb{R}, \end{aligned} \right\} \quad (11)$$

and

$$\left. \begin{aligned} \partial_t w &= f(w), & x \in \mathbb{R}, t > 0, \\ w(x, 0) &= w_0(x), & x \in \mathbb{R}. \end{aligned} \right\} \quad (12)$$

We denote by $X^t v_0$ and $Y^t w_0$, respectively, the solutions of (11) and (12). It is well known that for $t \geq 0$ and u_0 in $C_b^\infty(\mathbb{R})$, $\|X^t u_0\|_\infty \leq \|u_0\|_\infty$; furthermore property (10) holds naturally for Y^t with the assumption (9). The Lie approximation formulas are defined by

$$\mathcal{L}_1^t u_0 = X^t Y^t u_0, \quad \mathcal{L}_2^t u_0 = Y^t X^t u_0, \quad (13)$$

whereas the two Strang approximation formulas [40] are given by

$$\mathcal{S}_1^t u_0 = X^{t/2} Y^t X^{t/2} u_0, \quad \mathcal{S}_2^t u_0 = Y^{t/2} X^t Y^{t/2} u_0. \quad (14)$$

In what follows we investigate the error between the exact solution of equation (8), and the corresponding Lie approximations (13). Results for Strang local errors can be found in Appendix A. The Strang splitting approximation error for a semi-linear parabolic equation like (8) was also formally characterized in [21]. A different approach is adopted in the present study, where a more compact form of the representation of the error is considered to investigate its dependence on the initial condition and its derivatives. To perform these computations, we use formulas (6) and (7) from Corollary 1, and the Lie derivative calculus (see, for example, [19] Sect. III.5 or [24] Sect. IV.1.4 for an introduction to this topic). Lie calculus was also considered in [30, 9] and in [5] to study splitting schemes for, respectively, nonlinear Schrödinger equations and nonlinear reaction-diffusion equations. Notice that by considering equation (8) over \mathbb{R} , we exclude the boundary conditions from the present theoretical study. One must recall, however, that both Dirichlet and Neumann boundary conditions may have a negative influence on the splitting approximations, as previously mentioned in the Introduction (see, e.g., [23, 24, 22]). In particular, a recent study [15] mathematically investigates this problem for both Lie and Strang approximations applied to a two-dimensional inhomogeneous parabolic equation (similar to (8), but with $f(x, y, t)$, $(x, y) \in \mathbb{R}^2$, instead of $f(u)$).

Let us briefly recall in the following the definition and some properties of Lie derivatives. We consider function f as an unbounded nonlinear operator in $C_b^\infty(\mathbb{R})$. For any unbounded nonlinear operator G in $C_b^\infty(\mathbb{R})$ with Fréchet derivative G' , the corresponding Lie derivative D_f maps G to a new operator $D_f G$ such that for any u_0 in $C_b^\infty(\mathbb{R})$:

$$(D_f G)(u_0) = \partial_t G(Y^t u_0)|_{t=0} = G'(u_0)f(u_0).$$

Hence

$$(e^{tD_f} G)(u_0) = G(Y^t u_0),$$

and for $G = \text{Id}$, we have the following representation of the flow of (12):

$$(e^{tD_f} \text{Id})(u_0) = Y^t u_0.$$

Similarly, we can write the flow associated with (11) by considering the corresponding Lie derivative D_Δ . We finally recall that the commutator of Lie derivatives of two unbounded nonlinear operators is the Lie derivative of the Lie bracket of the unbounded nonlinear operators in reversed order. For instance, the Lie bracket for Δ and f is defined for any u_0 in $C_b^\infty(\mathbb{R})$ by

$$\begin{aligned} \{\Delta, f\}(u_0) &= \partial_x^2(f(u_0)) - f'(u_0)\partial_x^2 u_0 \\ &= f''(u_0)(\partial_x u_0, \partial_x u_0) = f''(u_0)(\partial_x u_0)^2, \end{aligned} \quad (15)$$

and thus we have

$$([D_f, D_\Delta] \text{Id})(u_0) = (D_{\{\Delta, f\}} \text{Id})(u_0) = \{\Delta, f\}(u_0).$$

Considering now the Lie splitting approximations (13) together with Lie derivative calculus, we have

$$T^t u_0 - \mathcal{L}_1^t u_0 = \left(e^{t(D_\Delta + D_f)} \text{Id} \right) (u_0) - \left(e^{tD_f} e^{tD_\Delta} \text{Id} \right) (u_0), \quad (16)$$

and

$$T^t u_0 - \mathcal{L}_2^t u_0 = \left(e^{t(D_\Delta + D_f)} \text{Id} \right) (u_0) - \left(e^{tD_\Delta} e^{tD_f} \text{Id} \right) (u_0), \quad (17)$$

which yield the following exact representations of the local error, denoted as

$$E_{\mathcal{L}_1}^t u_0 = T^t u_0 - X^t Y^t u_0, \quad E_{\mathcal{L}_2}^t u_0 = T^t u_0 - Y^t X^t u_0; \quad (18)$$

in which \mathcal{D} denotes the derivative with respect to the initial condition since T^t , X^t , and Y^t have been defined as semi flows.

Theorem 2. For $t \geq 0$ and u_0 in $C_b^\infty(\mathbb{R})$, we have

$$T^t u_0 - X^t Y^t u_0 = - \int_0^t \int_0^s \mathcal{D} T^{t-s} (X^s Y^s u_0) X^{s-r} f''(X^r Y^s u_0) (\partial_x X^r Y^s u_0)^2 dr ds, \quad (19)$$

and

$$\begin{aligned} T^t u_0 - Y^t X^t u_0 &= \int_0^t \int_0^s \mathcal{D} T^{t-s} (Y^s X^s u_0) \exp \left(\int_0^{s-r} f'(Y^{\sigma+r} X^s u_0) d\sigma \right) \times \\ &\quad f''(Y^r X^s u_0) \exp \left(2 \int_0^r f'(Y^\sigma X^s u_0) d\sigma \right) (\partial_x X^s u_0)^2 dr ds. \end{aligned} \quad (20)$$

Proof. Considering (6) we have

$$\begin{aligned} E_{\mathcal{L}_1}^t u_0 &= \left(e^{t(D_\Delta + D_f)} \text{Id} \right) (u_0) - \left(e^{tD_f} e^{tD_\Delta} \text{Id} \right) (u_0) \\ &= - \int_0^t \int_0^s \left(e^{sD_f} e^{rD_\Delta} [D_f, D_\Delta] e^{(s-r)D_\Delta} e^{(t-s)(D_\Delta + D_f)} \text{Id} \right) (u_0) dr ds \\ &= - \int_0^t \int_0^s \left(e^{rD_\Delta} [D_f, D_\Delta] e^{(s-r)D_\Delta} e^{(t-s)(D_\Delta + D_f)} \text{Id} \right) (Y^s u_0) dr ds \\ &= - \int_0^t \int_0^s \left(D_{\{\Delta, f\}} e^{(s-r)D_\Delta} e^{(t-s)(D_\Delta + D_f)} \text{Id} \right) (X^r Y^s u_0) dr ds \\ &= - \int_0^t \int_0^s \left(e^{(s-r)D_\Delta} e^{(t-s)(D_\Delta + D_f)} \text{Id} \right)' (X^r Y^s u_0) \{\Delta, f\} (X^r Y^s u_0) dr ds. \end{aligned}$$

Since $(e^{(s-r)D_\Delta} e^{(t-s)(D_\Delta + D_f)} \text{Id})(v_0) = T^{t-s} X^{s-r} v_0$, we obtain that

$$E_{\mathcal{L}_1}^t u_0 = - \int_0^t \int_0^s \mathcal{D} T^{t-s} (X^s Y^s u_0) \mathcal{D} X^{s-r} (X^r Y^s u_0) \{\Delta, f\} (X^r Y^s u_0) dr ds. \quad (21)$$

Formula (19) follows from (21) as a consequence of (15). By formally exchanging f and Δ (and thus Y and X) we infer from (17) and (6) that

$$E_{\mathcal{L}_2}^t u_0 = - \int_0^t \int_0^s \mathcal{D} T^{t-s} (Y^s X^s u_0) \mathcal{D} Y^{s-r} (Y^r X^s u_0) \{f, \Delta\} (Y^r X^s u_0) dr ds. \quad (22)$$

Given w_0 , the derivative of the solution of (12), $Y^s w_0(x)$, with respect to the initial condition, denoted by $\mathcal{D}Y^s(w_0)$, satisfies

$$\left. \begin{aligned} \partial_s \mathcal{D}Y^s(w_0) &= f'(Y^s w_0) \mathcal{D}Y^s(w_0), \\ \mathcal{D}Y^0(w_0) &= 1, \end{aligned} \right\}$$

and since f is a scalar function

$$\mathcal{D}Y^s(w_0) = \exp \left(\int_0^s f'(Y^\sigma w_0) d\sigma \right). \quad (23)$$

Similarly, $\partial_x Y^s w_0$ satisfies

$$\left. \begin{aligned} \partial_s \partial_x Y^s w_0 &= f'(Y^s w_0) \partial_x Y^s w_0, \\ \partial_x Y^0 w_0 &= \partial_x w_0, \end{aligned} \right\}$$

and hence

$$\partial_x Y^s w_0 = \exp \left(\int_0^s f'(Y^\sigma w_0) d\sigma \right) \partial_x w_0, \quad (24)$$

which along with (15) and (23) into (22), prove (20). \square

Notice that both error representations (4) and (6) are equivalent, nevertheless we will see in the following that the second one, used in Theorem 2, is more convenient because operators of type ∂_x are applied only on the split solutions $X^t v_0$ and $Y^t w_0$ of (11) and (12). A rigorous proof for (21) and (22) for two general nonlinear operators was also proposed in [9]. Furthermore, using Duhamel's formula we have for equation (8):

$$T^s u_0 = X^s u_0 + \int_0^s X^{s-r} f(T^r u_0) dr,$$

and hence

$$\mathcal{D}T^s(u_0) = X^s + \int_0^s X^{s-r} f'(T^r u_0) \mathcal{D}T^r(u_0) dr. \quad (25)$$

In particular using Gronwall's lemma we can also demonstrate that

$$\mathcal{D}T^s(u_0) = X^s \left(1 + \int_0^s f'(T^r u_0) \exp \left(\int_r^s X^{s-\sigma} f'(T^\sigma u_0) d\sigma \right) dr \right),$$

and hence have explicit expressions for both (19) and (20). We introduce now the following notation: for a scalar continuous function g and a real a , we denote

$$\|g\|_{[-a,a]} = \sup_{r \in [-a,a]} |g(r)|.$$

Using the results of Theorem 2, the following bounds can be obtained for both Lie local errors (16) and (17).

Theorem 3. For $t \in [0, T]$ and u_0 in $C_b^\infty(\mathbb{R})$, with $\kappa = \max(\|u_0\|_\infty, 1)$, we have

$$\|T^t u_0 - X^t Y^t u_0\|_\infty \leq \frac{t^2 \exp(2t\|f'\|_{[-\kappa,\kappa]}) \|f''\|_{[-\kappa,\kappa]}}{2} \|\partial_x u_0\|_\infty^2, \quad (26)$$

and

$$\|T^t u_0 - Y^t X^t u_0\|_\infty \leq \frac{t^2 \exp(2t\|f'\|_{[-\kappa,\kappa]}) \|f''\|_{[-\kappa,\kappa]}}{2} \|\partial_x u_0\|_\infty^2. \quad (27)$$

Proof. Taking norms for (21), we obtain

$$\begin{aligned} \|T^t u_0 - X^t Y^t u_0\|_\infty &\leq \int_0^t \int_0^s \|\mathcal{D}T^{t-s}(X^s Y^s u_0)\|_\infty \|f''(X^r Y^s u_0)\|_\infty \times \\ &\quad \left\| (\partial_x X^r Y^s u_0)^2 \right\|_\infty dr ds. \end{aligned}$$

From (25), assumption (9), and hence (10), we see that

$$\begin{aligned} \|\mathcal{D}T^s(u_0)\|_\infty &\leq 1 + \int_0^s \|f'(T^r u_0)\mathcal{D}T^r(u_0)\|_\infty dr \\ &\leq 1 + \int_0^s \|f'\|_{[-\kappa, \kappa]} \|\mathcal{D}T^r(u_0)\|_\infty dr. \end{aligned}$$

Gronwall's lemma then yields

$$\|\mathcal{D}T^s(u_0)\|_\infty \leq \exp(s\|f'\|_{[-\kappa, \kappa]}).$$

We thus have

$$\|T^t u_0 - X^t Y^t u_0\|_\infty \leq \int_0^t \int_0^s \exp((t-s)\|f'\|_{[-\kappa, \kappa]}) \|f''\|_{[-\kappa, \kappa]} \|\partial_x X^r Y^s u_0\|_\infty^2 dr ds. \quad (28)$$

Taking into account that $\|\partial_x X^r Y^s u_0\|_\infty^2 = \|X^r \partial_x Y^s u_0\|_\infty^2 \leq \|\partial_x Y^s u_0\|_\infty^2$ and with (24), we finally obtain

$$\begin{aligned} \|T^t u_0 - X^t Y^t u_0\|_\infty &\leq \int_0^t \int_0^s \exp((t+s)\|f'\|_{[-\kappa, \kappa]}) \|f''\|_{[-\kappa, \kappa]} \|\partial_x u_0\|_\infty^2 dr ds \\ &\leq \frac{t^2 \exp(2t\|f'\|_{[-\kappa, \kappa]}) \|f''\|_{[-\kappa, \kappa]}}{2} \|\partial_x u_0\|_\infty^2, \end{aligned}$$

which proves (26). The proof for (27) follows the same procedure which yields

$$\begin{aligned} \|T^t u_0 - Y^t X^t u_0\|_\infty &\leq \int_0^t \int_0^s \exp((t+r)\|f'\|_{[-\kappa, \kappa]}) \|f''\|_{[-\kappa, \kappa]} \|\partial_x X^s u_0\|_\infty^2 dr ds \\ &\leq \int_0^t \exp(2t\|f'\|_{[-\kappa, \kappa]}) \|f''\|_{[-\kappa, \kappa]} \|\partial_x X^s u_0\|_\infty^2 s ds, \end{aligned} \quad (29)$$

and proves (27) by considering that $\|\partial_x X^s u_0\|_\infty^2 = \|X^s \partial_x u_0\|_\infty^2 \leq \|\partial_x u_0\|_\infty^2$. \square

Notice that both Lie schemes are bounded by the same expression in Theorem 3, and for sufficiently small t these estimates involve the classical second order local error for Lie splitting. Considering now the Gauss-Weierstrass formula for the heat semi-group associated with (11), and the Young's inequality for convolutions, we have for all u_0 in $C_b^\infty(\mathbb{R})$ and $t > 0$, the following regularizing effect of the Laplace operator:

$$\|\partial_x X^t u_0\|_\infty \leq \frac{1}{\sqrt{\pi t}} \|u_0\|_\infty. \quad (30)$$

The following bounds can be then derived.

Theorem 4. For $t \in [0, T]$ and u_0 in $C_b^\infty(\mathbb{R})$, with $\kappa = \max(\|u_0\|_\infty, 1)$, we have

$$\|T^t u_0 - X^t Y^t u_0\|_\infty \leq \frac{4\kappa t \sqrt{t} \exp(t\|f'\|_{[-\kappa, \kappa]}) \|f''\|_{[-\kappa, \kappa]}}{3\sqrt{\pi}} \|\partial_x u_0\|_\infty \quad (31)$$

$$\|T^t u_0 - Y^t X^t u_0\|_\infty \leq \frac{2t\sqrt{t} \exp(2t\|f'\|_{[-\kappa, \kappa]}) \|f''\|_{[-\kappa, \kappa]}}{3\sqrt{\pi}} \|u_0\|_\infty \|\partial_x u_0\|_\infty, \quad (32)$$

and

$$\|T^t u_0 - Y^t X^t u_0\|_\infty \leq \frac{t \exp(2t\|f'\|_{[-\kappa, \kappa]}) \|f''\|_{[-\kappa, \kappa]}}{\pi} \|u_0\|_\infty^2. \quad (33)$$

Proof. Proof of (31) comes from considering the regularizing effect of the Laplacian (30) and that

$$\begin{aligned} \|\partial_x X^r Y^s u_0\|_\infty^2 &\leq \|\partial_x X^r Y^s u_0\|_\infty \|X^r \partial_x Y^s u_0\|_\infty \\ &\leq \frac{\max(\|u_0\|_\infty, 1) \times \exp(s\|f'\|_{[-\kappa, \kappa]}) \|\partial_x u_0\|_\infty}{\sqrt{\pi r}}, \end{aligned}$$

into (28), where assumption (9) has been considered and hence (10) for $\|Y^s u_0\|_\infty$. Similarly,

$$\|\partial_x X^s u_0\|_\infty^2 \leq \|\partial_x X^s u_0\|_\infty \|X^s \partial_x u_0\|_\infty \leq \frac{\|u_0\|_\infty \|\partial_x u_0\|_\infty}{\sqrt{\pi s}},$$

and

$$\|\partial_x X^s u_0\|_\infty^2 \leq \frac{\|u_0\|_\infty^2}{\pi s},$$

yield, respectively, (32) and (33) into (29). \square

Theorem 4 provides then with alternative estimates for both Lie methods. To summarize, and using the notation in (18) for a time t set by a given splitting time step Δt , we have the following results for u_0 in $C_b^\infty(\mathbb{R})$ and $\Delta t > 0$:

$$\|E_{\mathcal{L}_1}^{\Delta t} u_0\|_\infty \propto \min(\|\partial_x u_0\|_\infty^2 \Delta t^2, \max(\|u_0\|_\infty, 1) \times \|\partial_x u_0\|_\infty \Delta t^{1.5}),$$

and

$$\|E_{\mathcal{L}_2}^{\Delta t} u_0\|_\infty \propto \min(\|\partial_x u_0\|_\infty^2 \Delta t^2, \|u_0\|_\infty \|\partial_x u_0\|_\infty \Delta t^{1.5}, \|u_0\|_\infty^2 \Delta t).$$

For sufficiently small time steps, we thus recover the classical second order $\mathcal{O}(\Delta t^2)$ for local errors in accordance to the asymptotic behavior of both Lie splitting schemes. For larger time steps, however, the alternative estimates that behave like $\mathcal{O}(\Delta t^{1.5})$ or $\mathcal{O}(\Delta t)$ might become more relevant, which apparently entail a loss of accuracy of the splitting approximations. It is nevertheless important to highlight the impact of the multiplying constants in the different estimates, and in particular the nature of the initial condition and its derivatives, especially for non-asymptotic regimes defined by relatively large time step. Considering, for instance, solutions with high spatial gradients, the multiplying factor for the classical estimates in Δt^2 is of order $\mathcal{O}(\|\partial_x u_0\|_\infty^2)$, of smaller order $\mathcal{O}(\max(\|u_0\|_\infty, 1) \times \|\partial_x u_0\|_\infty)$ for $\Delta t^{1.5}$, and of potentially much smaller $\mathcal{O}(\|u_0\|_\infty^2)$ for Δt . Therefore, the alternative bounds given in Theorem 4 should describe much better the numerical behavior of the approximations, which in this case yield smaller local errors than those predicted by the classical estimates in Δt^2 , initially derived in Theorem 3. The same discussion is valid for the Strang local error estimates detailed in Appendix A.

3 Application to traveling waves

In this part we evaluate the previous theoretical study in the context of reaction-diffusion problems that admit self-similar traveling wave solutions. The main interest of considering this kind of configuration is that the featured stiffness can be tuned using a space-time scaling. Therefore, it provides the right framework to perform a complete numerical validation of the theoretical local error estimates. Moreover, a detailed study can be conducted on the impact of the stiffness featured by propagating fronts with steep spatial gradients as performed, for instance, in [11]. In what follows, we first recast previous estimates in the context of reaction traveling waves, and then we will illustrate them with the numerical solution of a KPP model.

3.1 Theoretical estimates

We consider the propagation of self-similar waves modeled by parabolic PDEs of type:

$$\left. \begin{aligned} \partial_t u - D \partial_x^2 u &= k f(u), & x \in \mathbb{R}, \ t > 0, \\ u(0, x) &= u_0(x), & x \in \mathbb{R}, \end{aligned} \right\} \quad (34)$$

with solution $u(x, t) = u_0(x - ct)$, where c is the steady speed of the wavefront, and D and k stand, respectively, for diffusion and reaction coefficients. Introducing the Lie splitting solutions (13) for equation (34) and taking into account that the corresponding Lie bracket is now defined as $\{D\Delta, kf\} = kD\{\Delta, f\}$, we obtain the following estimates.

Corollary 2. *For $t \in [0, T]$ and u_0 in $C_b^\infty(\mathbb{R})$, with $\kappa = \max(\|u_0\|_\infty, 1)$, we have*

$$\|T^t u_0 - X^t Y^t u_0\|_\infty \leq \frac{kD t^2 \exp(2kt\|f'\|_{[-\kappa, \kappa]}) \|f''\|_{[-\kappa, \kappa]}}{2} \|\partial_x u_0\|_\infty^2,$$

and

$$\|T^t u_0 - Y^t X^t u_0\|_\infty \leq \frac{kD t^2 \exp(2kt\|f'\|_{[-\kappa, \kappa]}) \|f''\|_{[-\kappa, \kappa]}}{2} \|\partial_x u_0\|_\infty^2.$$

Furthermore, with the regularizing effect of the Laplacian:

$$\|\partial_x X^t u_0\|_\infty \leq \frac{1}{\sqrt{\pi D t}} \|u_0\|_\infty,$$

the following bounds can be derived.

Corollary 3. *For $t \in [0, T]$ and u_0 in $C_b^\infty(\mathbb{R})$, with $\kappa = \max(\|u_0\|_\infty, 1)$, we have*

$$\|T^t u_0 - X^t Y^t u_0\|_\infty \leq \frac{4\kappa kD t \sqrt{t} \exp(kt\|f'\|_{[-\kappa, \kappa]}) \|f''\|_{[-\kappa, \kappa]}}{3\sqrt{\pi D}} \|\partial_x u_0\|_\infty$$

$$\|T^t u_0 - Y^t X^t u_0\|_\infty \leq \frac{2kD t \sqrt{t} \exp(2kt\|f'\|_{[-\kappa, \kappa]}) \|f''\|_{[-\kappa, \kappa]}}{3\sqrt{\pi D}} \|u_0\|_\infty \|\partial_x u_0\|_\infty,$$

and

$$\|T^t u_0 - Y^t X^t u_0\|_\infty \leq \frac{k t \exp(2kt\|f'\|_{[-\kappa, \kappa]}) \|f''\|_{[-\kappa, \kappa]}}{\pi} \|u_0\|_\infty^2.$$

In the context of traveling wave solutions, the diffusion and reaction coefficients, D and k , might be seen as scaling coefficients in time and space. A dimensionless analysis of a traveling wave can be then conducted, as shown in [18], by considering dimensionless time τ and space r :

$$\tau = kt, \quad r = (k/D)^{1/2} x.$$

As a consequence, a steady velocity of the wavefront can be derived

$$c = d_t x \propto (Dk)^{1/2}, \quad (35)$$

whereas the sharpness of the wave profile is measured by

$$d_x u_0|_{\max} = \|\partial_x u_0\|_\infty \propto (k/D)^{1/2}. \quad (36)$$

Condition $Dk = 1$ then involves waves of constant velocity, but greater k (or smaller D) yields wavefronts with higher spatial gradients, and thus stiffer configurations.

By considering the Lie local errors (18) for a time t set by a given splitting time step Δt , the bounds from Corollary 2 and 3, and the measure of the wave gradient (36) together with condition $Dk = 1$, we have that for u_0 in $C_b^\infty(\mathbb{R})$ and $\Delta t > 0$:

$$\|E_{\mathcal{L}_1}^{\Delta t} u_0\|_\infty \propto \min(k^2 \Delta t^2, \max(\|u_0\|_\infty, 1) \times k^{1.5} \Delta t^{1.5}),$$

and

$$\|E_{\mathcal{L}_2}^{\Delta t} u_0\|_\infty \propto \min(k^2 \Delta t^2, \|u_0\|_\infty k^{1.5} \Delta t^{1.5}, \|u_0\|_\infty^2 k \Delta t).$$

Even though these bounds are not sufficient to determine precisely the various intervals of numerical behavior depending on Δt , *i.e.*, the actual time steps for which each bound becomes relevant, for solutions with high spatial gradients it is very likely to start having transitions from one behavioral regime to another even for small splitting time steps of about $\|\partial_x u_0\|_\infty^{-1}$ (or k^{-1} following (36) with $Dk = 1$), based on a simple comparison of the multiplying coefficients in the estimates. Similar conclusions can be drawn from Strang local error estimates.

3.2 Numerical illustration: 1D KPP equation

Recalling the classical Kolmogorov-Petrovskii-Piskunov model [27] with $f(u) = u(1 - u)$, we consider in this study a higher order KPP nonlinearity with $f(u) = u^2(1 - u)$ (often referred to as Zeldovich nonlinearity). The description of the dimensionless model and the structure of the analytical solution for this case can be found, for instance, in [18], where a theoretical analysis shows that in the case with $D = k = 1$, the velocity of the self-similar traveling wave is $c = 1/\sqrt{2}$ in (35), and the maximum gradient value reaches $1/\sqrt{32}$ in (36). Notice that for this KPP nonlinearity there is a single isolated value of the speed for which the front exists, contrary to the monostable, classical KPP equation. In particular the case $f(u) = u^2(1 - u)$ verifies assumption (9) on $f(u)$, considered in §2.2. The key point of this illustration is that the velocity of the traveling wave is proportional to $(kD)^{1/2}$, whereas the maximum gradient is proportional to $(k/D)^{1/2}$. Hence, we consider the case $kD = 1$ for which one may obtain steeper gradients with the same speed of propagation.

For the numerical approximations, we consider a 1D discretization with 5001 points over a region of $[-70, 70]$ with homogeneous Neumann boundary conditions, for which we have negligible spatial discretization errors with respect to the ones coming from the numerical time integration for the relatively large time steps that have been considered. The Laplacian is discretized using a standard second order, centered finite differences scheme. The exact solution $T^t u_0$ will be approximated by a reference or *quasi-exact* solution given by the numerical solution of the coupled reaction-diffusion equation performed by the Radau5 solver [20] with a fine tolerance, $\eta_{\text{Radau5}} = 10^{-10}$. Notice that even though an analytic solution exists, we consider a reference solution corresponding to the semi-discretized problem in order to avoid including spatial discretization errors in the analysis, that is, both the reference and splitting solutions are computed on the same grid with the same spatial discretization. All splitting approximations are computed with the splitting technique introduced in [12], with Radau5 for the reactive term, and the ROCK4 method [1] for the diffusion problem. In order to properly discriminate splitting errors from those coming from the temporal integration of the subproblems, we consider the following fine tolerances, $\eta_{\text{Radau5}} = \eta_{\text{ROCK4}} = 10^{-10}$. For this particular problem another option for the splitting approximation might have taken into account the ODE analytic solution for the reaction steps, as well as the solution of the discrete heat equation for the diffusion subproblems by considering, for instance, Fast Fourier Transforms (FFT). However, a fully numerical approach is adopted in this study in accordance with more general and complex configurations envisioned, as the ones presented in [10, 13] and in the next section. Figure 1 shows the numerical *quasi-exact* solutions at times $t = 0$ and $t = 45$ for $k = 1, 10$, and 100 . In what follows, 10001 points of discretization are considered for $k = 100$ instead of 5001 in order to better represent the wavefront, as illustrated in Figure 1.

We first compute the L^2 local errors for different splitting time steps Δt for all Lie and Strang splitting schemes, that is, $\mathcal{L}_1^{\Delta t}$, $\mathcal{L}_2^{\Delta t}$, $\mathcal{S}_1^{\Delta t}$, and $\mathcal{S}_2^{\Delta t}$ in (13) and (14). Starting from the same initial

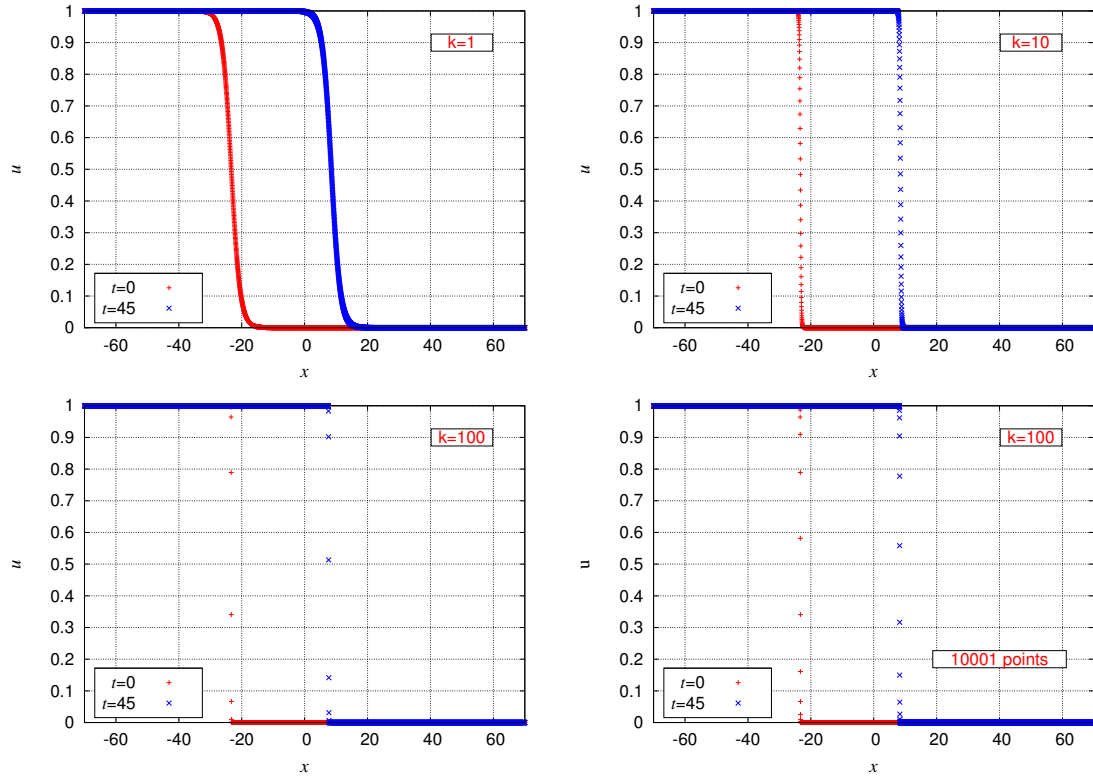


Figure 1: 1D KPP. Numerical *quasi-exact* solutions at $t = 0$ and $t = 45$ for $k = 1$ (top left), 10 (top right) and 100 (bottom left) with a discretization of 5001 points. Bottom right: case $k = 100$ with 10001 points of discretization.

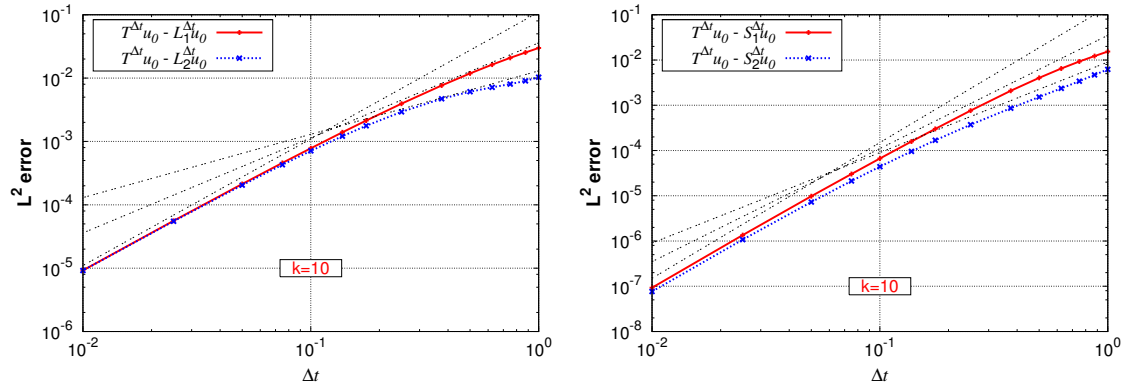


Figure 2: 1D KPP with $k = 10$. Local L^2 errors for several splitting time steps Δt for Lie (left) and Strang (right) splitting schemes. Dashed lines with slopes 2, 1.5, and 1 (left), and with 3, 2.5, and 2 (right) are depicted.

solution u_0 , the local error associated with $\mathcal{L}_1^{\Delta t} u_0$ is measured by $\|T^{\Delta t} u_0 - \mathcal{L}_1^{\Delta t} u_0\|_{L^2}$, and similarly for the other schemes. Figure 2 illustrates these errors for $k = 10$, for relatively large splitting

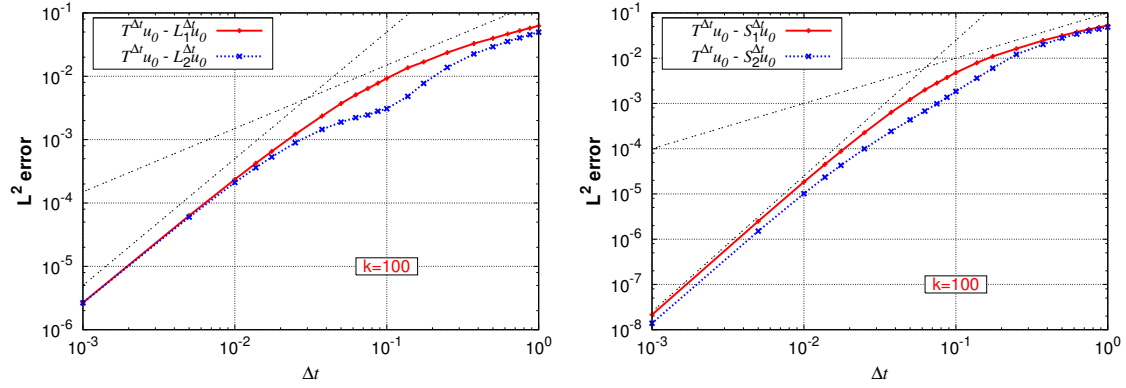


Figure 3: 1D KPP with $k = 100$. Local L^2 errors for several splitting time steps Δt for Lie (left) and Strang (right) splitting schemes. Dashed lines with slopes 2 and 1 (left), and with 3 and 1 (right) are depicted.

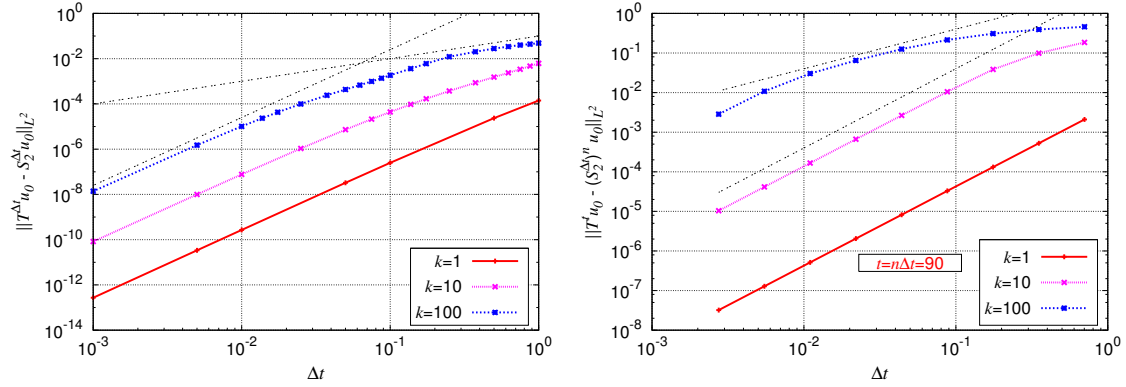


Figure 4: 1D KPP. \mathcal{S}_2 -Strang local (left) and global (right) L^2 errors for several splitting time steps Δt and $k = 1, 10$, and 100 . Dashed lines with slopes 3 and 1 (left), and with 2 and 1 (right) are depicted.

time steps. A deviation from the asymptotic behavior is exhibited for all splitting schemes for time steps of order k^{-1} or larger. For smaller time steps we retrieve classical orders as established in Theorems 3 and 6. In this case, \mathcal{L}_1 - and \mathcal{L}_2 -Lie schemes are practically equivalent in terms of accuracy, as established in Theorem 3. On the other hand, there is a slight difference for \mathcal{S}_1 - and \mathcal{S}_2 -Strang schemes, as seen in Theorem 6. For the \mathcal{L}_1 -Lie scheme, the dependence on Δt varies from Δt^2 to $\Delta t^{1.5}$, whereas it attains Δt for the \mathcal{L}_2 -Lie scheme, as described in Theorem 4. For the Strang schemes, the same phenomenon occurs from Δt^3 to $\Delta t^{2.5}$ and Δt^2 , respectively, for the \mathcal{S}_1 - and \mathcal{S}_2 -Strang schemes, following the bounds established in Theorem 7. Notice that in all cases a better accuracy is achieved in the non-asymptotic regime by splitting schemes ending with the reaction substep, as previously proved in [7]. In particular the \mathcal{L}_2 -Lie scheme is even more accurate than a \mathcal{S}_1 -Strang one, for sufficiently large splitting time steps. Similar conclusions are drawn for a stiffer configuration with $k = 100$, illustrated in Figure 3. In this case the splitting local errors eventually behave like Δt . In this way the bounds introduced in Theorems 4 and 7, as well as the mathematical characterization of these errors for non-asymptotic regimes, consistently describe the

numerical accuracy of operator splitting for solutions disclosing high spatial gradients. Considering the global error for the \mathcal{S}_2 -Strang scheme: $\|T^t u_0 - (\mathcal{S}_2^{\Delta t})^n u_0\|_{L^2}$, where $\mathcal{S}_2^{\Delta t}$ has been successively applied n times to u_0 , such that $t = n\Delta t$, Figure 4 illustrates these errors for the \mathcal{S}_2 -Strang scheme, which perfectly reproduces the behavior of local errors. The latter is not always the case since there might be some error compensation and thus a global accuracy better than the one theoretically expected. This has been shown, for instance, in [25] for a linear configuration but the proofs cannot be extended to a nonlinear framework. In particular the global error evaluation in Figure 4 was made after a long integration time in order to illustrate the worst possible configuration. The influence of stiffness is highlighted for increasingly stiffer configurations corresponding to higher values of k . Notice that for $k = 1$, a non-stiff configuration, asymptotic orders are preserved even for relatively large splitting time steps.

4 Application to the dynamics of premixed flames

We now consider the simulation of a counterflow premixed methane flame with detailed transport and complex chemistry in the low Mach number regime. These flames have received an extensive number of studies in both the steady and the pulsated case for realistic engineering applications (see *e.g.*, [37, 16, 29]). Here we will consider the configuration where the flame is pulsated periodically in time through upstream modulations [3]. In this way we consider a time dependent system of PDEs for which we introduce a new way to perform operator splitting, compatible with the low Mach constraint. Taking into account that there is already a validated coupled, fully implicit code, based on [3, 33], that can provide us with the reference dynamics of such flames, we evaluate the splitting errors introduced by this new approach and analyze the resulting behavior based on the theoretical study previously conducted.

4.1 Governing equations

We consider two premixed flames stabilized in a symmetric framework where two injections of methane-air mixture occur in a counterflow way (see Figure 9 in Appendix B). Isobaric flames equations are considered in the low Mach Number limit [31], so that for $\mathbf{x} \in \mathbb{R}^d$ the pressure reads $p(t, \mathbf{x}) = p_{atm} + \tilde{p}(t, \mathbf{x})$, where \tilde{p} is a perturbation of the atmospheric pressure. The counterflow configuration admits a symmetry of revolution and thus the set of equations can be written as a 2D axisymmetric system. In particular, we consider 1D similarity solutions of this 2D system of equations for which the density of the gas ρ , the temperature T , the axial velocity u_z , the reduced radial velocity u_r/r , and the mass fractions Y_k of the gas species have no radial dependence, and all of them are functions of the axial coordinate z . Assuming that the perturbation on the atmospheric pressure field is given by $\tilde{p} = -Jr^2/2 + \hat{p}(z)$, where r denotes the radial coordinate, the governing equations read

$$\rho c_p \partial_t T + c_p V \partial_z T - \partial_z (\lambda \partial_z T) = - \sum_{k \in S} h_k m_k \omega_k - \sum_{k \in S} \rho Y_k c_{p,k} \mathcal{V}_{z,k} \partial_z T, \quad (37)$$

$$\rho \partial_t Y_k + V \partial_z Y_k + \partial_z (\rho Y_k \mathcal{V}_{z,k}) = m_k \omega_k, \quad k \in S, \quad (38)$$

$$\partial_z J = 0, \quad (39)$$

$$\rho \partial_t U + \rho U^2 + V \partial_z U = J + \partial_z (\mu \partial_z U), \quad (40)$$

$$\partial_t \rho + 2\rho U + \partial_z V = 0, \quad (41)$$

where $V = \rho u_z$ is the axial mass flux, U the reduced radial velocity, S the set of species indices, c_p the specific heat of the gas mixture, $c_p = \sum_{k \in S} Y_k c_{p,k}$, $c_{p,k}$ the specific heat of the k -th species, h_k its enthalpy, m_k its molar mass, λ the heat conductivity, μ the shear viscosity, J the reduced

pressure gradient, ω_k the molar chemical production rate, and $\mathcal{V}_{k,z}$ the axial diffusion velocity of the k -th gas species. Density ρ is a function of the local temperature and gas composition through the ideal gas state equation. Full details on this model can be found, for instance, in [17].

Given the symmetry of this configuration, only half domain is considered, $z \geq 0$, with symmetry conditions at $z = 0$. The top boundary at $z = 1.55$ cm coincides with the fuel injection and thus fixed values of the temperature, the axial and the reduced radial velocities, and the gas composition are imposed. Its velocity is of 1.423 m/s, pulsated with a modulation of 10% at a frequency of 100 Hz. The gas is composed of methane with a mass fraction equal to 3.88%, mixed with air at 293 K and atmospheric pressure. A detailed methane-air chemical kinetic mechanism with 29 species and 150 reactions is considered, whereas transport parameters are computed based on [14].

4.2 Introduction of operator splitting

We aim at solving separately the chemical sources in system (37)–(41):

$$\rho c_p \partial_t T = - \sum_{k \in S} h_k m_k \omega_k, \quad (42)$$

$$\rho \partial_t Y_k = m_k \omega_k, \quad k \in S, \quad (43)$$

and then consider the following convection-diffusion problem:

$$\rho c_p \partial_t T + c_p V \partial_z T - \partial_z (\lambda \partial_z T) = - \sum_{k \in S} \rho Y_k c_{p,k} \mathcal{V}_{z,k} \partial_z T, \quad (44)$$

$$\rho \partial_t Y_k + V \partial_z Y_k + \partial_z (\rho Y_k \mathcal{V}_{z,k}) = 0, \quad k \in S, \quad (45)$$

$$\partial_z J = 0, \quad (46)$$

$$\rho \partial_t U + \rho U^2 + V \partial_z U = J + \partial_z (\mu \partial_z U), \quad (47)$$

$$\partial_t \rho + 2\rho U + \partial_z V = 0. \quad (48)$$

In this way, we obtain a decoupled system of ODEs (42)–(43) on each grid point of the domain, for which a dedicated stiff ODE solver can be implemented; whereas the numerical effort required to solve the coupled system (44)–(48) is also relieved. However, since density ρ depends on the local temperature and gas composition, its time variation during the chemistry step (42)–(43) must be taken into account in equation (48). Deriving in time the ideal gas state equation and considering (42)–(43), this variation, denoted as $(\partial_t \rho)_{\text{chem}}$, is given by

$$(\partial_t \rho)_{\text{chem}} = \frac{1}{c_p T} \sum_{k \in S} h_k m_k \omega_k - m \sum_{k \in S} \omega_k. \quad (49)$$

Hydrodynamics are therefore solved, coupled with the transport equations without chemical source terms for temperature and species, in system (44)–(47) together with

$$\partial_t \rho + (\partial_t \rho)_{\text{chem}} + 2\rho U + \partial_z V = 0, \quad (50)$$

instead of (48).

In this implementation, the corrective term $(\partial_t \rho)_{\text{chem}}$ is updated at the beginning of each splitting time step, and kept constant throughout the time integration of the current time step. Considering the instantaneous nature of this correction that affects especially the solution of the hydrodynamics, both Lie and Strang schemes should finish with the numerical solution of the convection-diffusion problem (44)–(47) plus (50). This is also coherent with the idea of always ending the splitting scheme with the fastest operator [38, 28, 7]. The convection-diffusion system

is numerically solved with the same code considered for the original full problem (37)–(41). The method considers implicit time integration of the coupled equations on a dynamically adapted grid (see details in [37, 3]). On the other hand, the chemical source terms (42)–(43) are integrated point-wise with the Radau5 solver [20].

4.3 Numerical results

To visualize the numerical performance of the splitting approximation, the point $z = 0.25$ cm in the high gradient zone is chosen (see Figure 10). The evolution of the temperature is shown in Figure 5 for Lie and Strang approximations with different splitting time steps. The reference solution corresponds to the solution of the full problem (37)–(41), computed with fine tolerances (see [37]). For the time steps considered the dynamics of the flame is properly reproduced with the new operator splitting introduced. The same can be observed even for minor species, as illustrated, for instance, in Figure 6 for Y_{OH} .

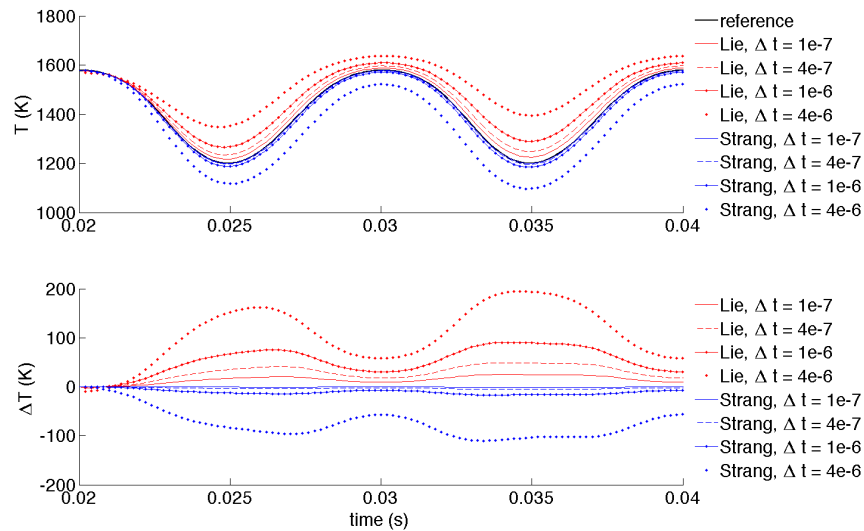


Figure 5: Top: time evolution of temperature at point $z = 0.25$ cm, with the reference solution (black line), and the Lie (blue lines) and Strang (red lines) splitting approximations. Bottom: difference with respect to the reference solution with $\Delta t = 10^{-7}$.

Figures 7 and 8 illustrate the local and global errors for the Lie and Strang splitting approximations, respectively, for relatively large splitting time steps. We consider temperature T , and some main and minor species like Y_{CH_4} and Y_{CO_2} , and Y_{OH} and Y_{CH} , respectively. Global errors are evaluated at time 0.032s, which corresponds to a maximum pulsated velocity. For the Lie approximations, the dependence on the splitting time step Δt varies from Δt^2 to $\Delta t^{1.5}$ (close to Δt for Y_{CH}); and similarly from Δt^3 to $\Delta t^{2.5}$, for the Strang solutions in Figure 8 (about Δt^2 for Y_{CH}). Global errors follow approximately the same behaviors. However, compensations can take place as illustrated, for instance, by the Strang scheme that displays behaviors between Δt^2 and $\Delta t^{1.5}$, even for very large splitting time steps. The Lie scheme on the other side involves a global accuracy that behaves like $\Delta t^{0.5}$, and even worse for very large time steps. In what concerns to the present study we can identify similar behaviors previously observed for the KPP problem, and predicted by the theoretical study, this time for a much more complex problem. In particular splitting approximations with relatively large time steps involve better accuracies than those expected out of the asymptotic bounds. Moreover, splitting errors remain bounded even for considerably large time

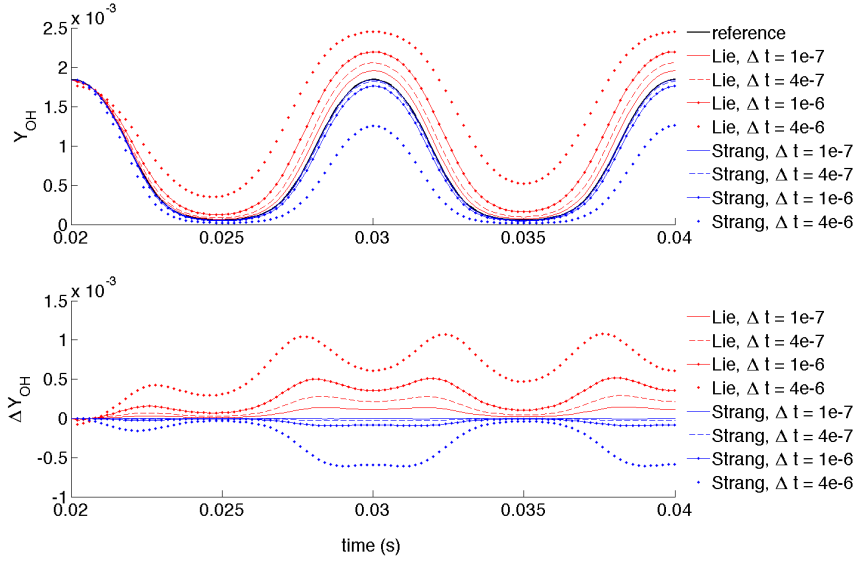


Figure 6: Top: time evolution of the mass fraction of OH at point $z = 0.25$ cm with the reference solution (black line), and the Lie (blue lines) and Strang (red lines) splitting approximations. Bottom: difference with respect to the reference solution with $\Delta t = 10^{-7}$.

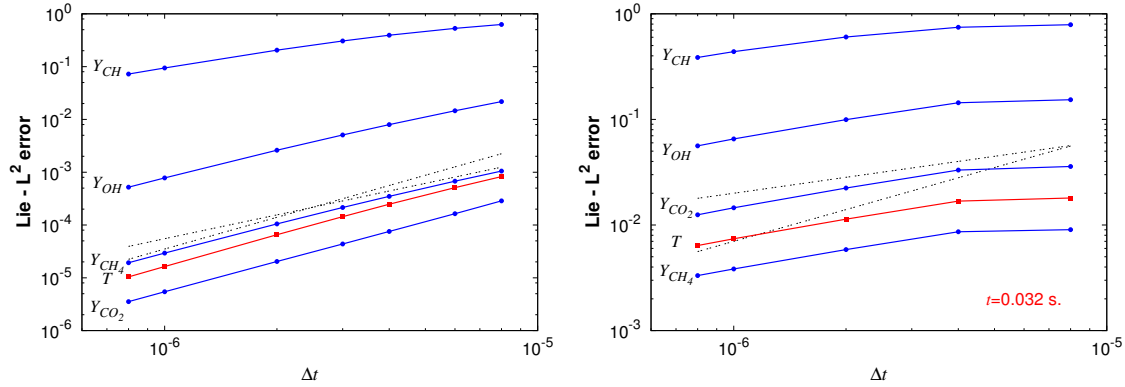


Figure 7: Local (left) and global (right) L^2 errors for the Lie scheme for temperature T and species Y_{CH_4} , Y_{CO_2} , Y_{OH} , and Y_{CH} . Lines with slope of 2 and 1.5 (left), and of 1 and 0.5 (right) are depicted.

steps of about 10^{-5} s, compared, for instance, with some of the chemical time scales, of the order of the nanoseconds. Complementary analyses on these numerical results, as well as more details and further extensions of this approach for Low Mach number flames will be reported in a forthcoming work.

5 Concluding remarks

We have introduced in this paper a rigorous mathematical characterization of splitting errors for nonlinear reaction-diffusion equations. The corresponding error estimates are particularly relevant for relatively large splitting time steps, and therefore for many applications modeled by stiff PDEs in which fast physical or numerical scales usually impose prohibitively expensive time steps. In this

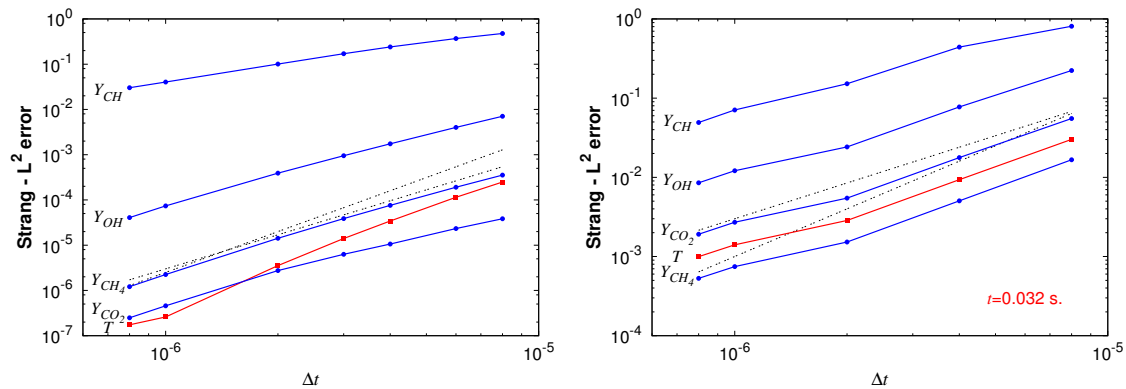


Figure 8: Local (left) and global (right) L^2 errors for the Strang scheme for temperature T and species Y_{CH_4} , Y_{CO_2} , Y_{OH} , and Y_{CH} . Lines with slope of 3 and 2.5 (left), and of 2 and 1.5 (right) are depicted.

context splitting techniques can become a more efficient alternative to overcome stability restrictions related to stiff source terms or mesh size, as shown in [12]. Additionally, a theoretical description of splitting errors may also lead to further developments, as the adaptive splitting scheme introduced in [5]. Understanding the numerical behavior of splitting schemes, especially for relatively large splitting time steps, is therefore shown to be of the utmost importance for both theoretical and practical reasons. Besides, we have illustrated the relevance of the present theoretical study in the case of self-similar waves with high spatial gradients. This kind of problem mimics many other applications characterized by the propagation of steep chemical fronts. In particular we have considered a counterflow premixed flame with complex chemistry and detailed transport, for which we have also introduced a new way of implementing operator splitting techniques. In all cases the key point of these numerical illustrations is that the present theoretical study consistently describes the behavior of the numerical errors, especially for relatively large splitting time steps. It can be thus seen how better accuracies are actually achieved with respect to the asymptotic bounds in the case of propagating fronts with steep spatial gradients.

Acknowledgements

This research was supported by an ANR project grant (French National Research Agency - ANR Blancs): *Séchelles* (PI S. Descombes - 2009-2013), by a DIGITEO RTRA project: *MUSE* (PI M. Massot - 2010-2014), and by a France-Stanford project (PIs P. Moin & M. Massot - 2011-2012). M. Duarte was partially supported by the Applied Mathematics Program of the DOE Office of Advance Scientific Computing Research under contract No. DE-AC02-05CH11231 at LBNL.

A Local error estimates for Strang splitting

Based on formula (7) we can also obtain an exact representation of Strang local errors, considering the same type of computations carried out for the proof of Theorem 2 and taking into account that

$$\begin{aligned} ([D_f, [D_f, D_\Delta]]\text{Id})(u_0) = & f^{(3)}(u_0) (\partial_x u_0, \partial_x u_0, f(u_0)) + 2f''(u_0) (\partial_x u_0, f'(u_0) \partial_x u_0) \\ & - f'(u_0) f''(u_0) (\partial_x u_0, \partial_x u_0), \end{aligned} \quad (51)$$

and

$$\begin{aligned} ([D_\Delta, [D_\Delta, D_f]] \text{Id}) (u_0) &= f^{(4)}(u_0) (\partial_x u_0, \partial_x u_0, \partial_x u_0, \partial_x u_0) \\ &\quad + 4f^{(3)}(u_0) (\partial_x u_0, \partial_x u_0, \partial_x^2 u_0) + 2f''(u_0) (\partial_x^2 u_0, \partial_x^2 u_0). \end{aligned} \quad (52)$$

Theorem 5. For $t \geq 0$ and u_0 in $C_b^\infty(\mathbb{R})$, we have

$$\begin{aligned} T^t u_0 - X^{t/2} Y^t X^{t/2} u_0 &= -\frac{1}{4} \int_0^t \int_0^s (s-r) \mathcal{D} T^{t-s} (X^{s/2} Y^s X^{s/2} u_0) X^{(s-r)/2} \times \\ &\quad ([D_\Delta, [D_\Delta, D_f]] \text{Id}) (X^{r/2} Y^s X^{s/2} u_0) dr ds \\ &\quad + \frac{1}{2} \int_0^t \int_0^s (s-r) \mathcal{D} T^{t-s} (X^{s/2} Y^s X^{s/2} u_0) X^{s/2} \times \\ &\quad \exp \left(\int_0^r f'(Y^{\sigma+s-r} X^{s/2} u_0) d\sigma \right) \times \\ &\quad ([D_f, [D_f, D_\Delta]] \text{Id}) (Y^{s-r} X^{s/2} u_0) dr ds \end{aligned} \quad (53)$$

and

$$\begin{aligned} T^t u_0 - Y^{t/2} X^t Y^{t/2} u_0 &= -\frac{1}{4} \int_0^t \int_0^s (s-r) \mathcal{D} T^{t-s} (Y^{s/2} X^s Y^{s/2} u_0) \times \\ &\quad \exp \left(\int_0^{(s-r)/2} f'(Y^{\sigma+r/2} X^s Y^{s/2} u_0) d\sigma \right) \times \\ &\quad ([D_f, [D_f, D_\Delta]] \text{Id}) (Y^{r/2} X^s Y^{s/2} u_0) dr ds \\ &\quad + \frac{1}{2} \int_0^t \int_0^s (s-r) \mathcal{D} T^{t-s} (Y^{s/2} X^s Y^{s/2} u_0) \times \\ &\quad \exp \left(\int_0^{s/2} f'(Y^\sigma X^s Y^{s/2} u_0) d\sigma \right) X^r \times \\ &\quad ([D_\Delta, [D_\Delta, D_f]] \text{Id}) (X^{s-r} Y^{s/2} u_0) dr ds \end{aligned} \quad (54)$$

The following bounds can be then obtained for the local errors corresponding to both Strang approximations (14), following the procedure considered for the proof of Theorem 3 for (53)–(54) together with (51)–(52).

Theorem 6. For $t \in [0, T]$ and u_0 in $C_b^\infty(\mathbb{R})$, with $\kappa = \max(\|u_0\|_\infty, 1)$, we have

$$\begin{aligned} \|T^t u_0 - X^{t/2} Y^t X^{t/2} u_0\|_\infty &\leq \\ &\left[\frac{t^3 \|f^{(4)}\|_{[-\kappa, \kappa]}}{24} + \frac{t^4 \|f^{(3)}\|_{[-\kappa, \kappa]} \|f''\|_{[-\kappa, \kappa]}}{8} + \frac{t^5 \|f''\|_{[-\kappa, \kappa]}^3}{20} \right] \exp(4t \|f'\|_{[-\kappa, \kappa]}) \|\partial_x u_0\|_\infty^4 \\ &+ \left[\frac{t^3 \|f^{(3)}\|_{[-\kappa, \kappa]}}{6} + \frac{t^4 \|f''\|_{[-\kappa, \kappa]}^2}{8} \right] \exp(3t \|f'\|_{[-\kappa, \kappa]}) \|\partial_x u_0\|_\infty^2 \|\partial_x^2 u_0\|_\infty \\ &+ \frac{t^3 \exp(2t \|f'\|_{[-\kappa, \kappa]}) \|f''\|_{[-\kappa, \kappa]}}{12} \|\partial_x^2 u_0\|_\infty^2 \\ &+ \frac{t^3 \exp(2t \|f'\|_{[-\kappa, \kappa]}) [\|f'\|_{[-\kappa, \kappa]} \|f''\|_{[-\kappa, \kappa]} + \|f\|_{[-\kappa, \kappa]} \|f^{(3)}\|_{[-\kappa, \kappa]}}{12} \|\partial_x u_0\|_\infty^2, \end{aligned}$$

and

$$\begin{aligned}
& \left\| T^t u_0 - Y^{t/2} X^t Y^{t/2} \right\|_\infty \leq \\
& \left[\frac{t^3 \|f^{(4)}\|_{[-\kappa, \kappa]}}{12} + \frac{t^4 \|f^{(3)}\|_{[-\kappa, \kappa]} \|f''\|_{[-\kappa, \kappa]}}{8} + \frac{t^5 \|f''\|_{[-\kappa, \kappa]}^3}{40} \right] \exp(2.5t \|f'\|_{[-\kappa, \kappa]}) \|\partial_x u_0\|_\infty^4 \\
& + \left[\frac{t^3 \|f^{(3)}\|_{[-\kappa, \kappa]}}{3} + \frac{t^4 \|f''\|_{[-\kappa, \kappa]}^2}{8} \right] \exp(2t \|f'\|_{[-\kappa, \kappa]}) \|\partial_x u_0\|_\infty^2 \|\partial_x^2 u_0\|_\infty \\
& + \frac{t^3 \exp(1.5t \|f'\|_{[-\kappa, \kappa]}) \|f''\|_{[-\kappa, \kappa]}}{6} \|\partial_x^2 u_0\|_\infty^2 \\
& + \frac{t^3 \exp(2t \|f'\|_{[-\kappa, \kappa]}) [\|f'\|_{[-\kappa, \kappa]} \|f''\|_{[-\kappa, \kappa]} + \|f\|_{[-\kappa, \kappa]} \|f^{(3)}\|_{[-\kappa, \kappa]}]}{24} \|\partial_x u_0\|_\infty^2.
\end{aligned}$$

Considering the regularizing effects of the Laplacian (30) and

$$\|\partial_x^2 X^t u_0\|_\infty \leq \frac{1}{t} \|u_0\|_\infty,$$

the next theorem yields alternative estimates as in Theorem 4 for the Lie case.

Theorem 7. For $t \in (0, T)$ and u_0 in $C_b^\infty(\mathbb{R})$, with $\kappa = \max(\|u_0\|_\infty, 1)$, we have

$$\begin{aligned}
& \left\| T^t u_0 - X^{t/2} Y^t X^{t/2} \right\|_\infty \leq \\
& \frac{t \exp(4t \|f'\|_{[-\kappa, \kappa]}) [\|f^{(4)}\|_{[-\kappa, \kappa]} \|u_0\|_\infty^4 + 4\pi \|f^{(3)}\|_{[-\kappa, \kappa]} \|u_0\|_\infty^3 + 2\pi^2 \|f''\|_{[-\kappa, \kappa]} \|u_0\|_\infty^2]}{2\pi^2} \\
& + \frac{t^2 \exp(4t \|f'\|_{[-\kappa, \kappa]}) [\|f^{(3)}\|_{[-\kappa, \kappa]} \|f''\|_{[-\kappa, \kappa]} \|u_0\|_\infty^4 + \pi \|f''\|_{[-\kappa, \kappa]}^2 \|u_0\|_\infty^3]}{\pi^2} \\
& + \frac{t^2 \exp(2t \|f'\|_{[-\kappa, \kappa]}) [\|f'\|_{[-\kappa, \kappa]} \|f''\|_{[-\kappa, \kappa]} + \|f\|_{[-\kappa, \kappa]} \|f^{(3)}\|_{[-\kappa, \kappa]}] \|u_0\|_\infty^2}{4\pi} \\
& + \frac{t^3 \exp(4t \|f'\|_{[-\kappa, \kappa]}) \|f''\|_{[-\kappa, \kappa]}^3 \|u_0\|_\infty^4}{3\pi^2}.
\end{aligned}$$

and

$$\begin{aligned}
& \left\| T^t u_0 - Y^{t/2} X^t Y^{t/2} \right\|_\infty \leq \\
& \frac{\kappa t \sqrt{t} \exp(t \|f'\|_{[-\kappa, \kappa]}) [2\kappa^2 \|f^{(4)}\|_{[-\kappa, \kappa]} + 8\pi \kappa \|f^{(3)}\|_{[-\kappa, \kappa]} + 4\pi \|f''\|_{[-\kappa, \kappa]}]}{3\pi \sqrt{\pi}} \|\partial_x u_0\|_\infty \\
& + \frac{\kappa^2 t^2 \exp(1.5t \|f'\|_{[-\kappa, \kappa]}) [\|f'\|_{[-\kappa, \kappa]} \|f''\|_{[-\kappa, \kappa]} + \|f\|_{[-\kappa, \kappa]} \|f^{(3)}\|_{[-\kappa, \kappa]}]}{16\pi}.
\end{aligned}$$

Notice that the previous bounds are derived by using the regularizing effects of the Laplacian as much as possible. Additional bounds could be nevertheless derived (similar to (32) in Theorem 4) of $\mathcal{O}(t^{2.5})$, $\mathcal{O}(t^2)$, and $\mathcal{O}(t^{1.5})$ for the \mathcal{S}_1 -Strang scheme, and of $\mathcal{O}(t^{2.5})$ and $\mathcal{O}(t^2)$ for the \mathcal{S}_2 -Strang splitting.

B Laminar premixed counterflow flame

The counterflow, premixed methane flame configuration is illustrated in Figure 9. Two premixed flames are stabilized between two injections of the same mixture of methane and air with an axial

velocity of 1.423 m/s. These jets are pulsed with a frequency of 100 Hz and a modulation of 10%, in a synchronized way, so that the plane $z = 0$ remains in the symmetry plane. The distance between the injectors and this stagnation planes is $d = 1.55$ cm. Figure 10 illustrates the velocity pulsations on the fuel injection, and the time variations of temperature profiles, as well as for Y_{CH_4} and Y_{OH} .

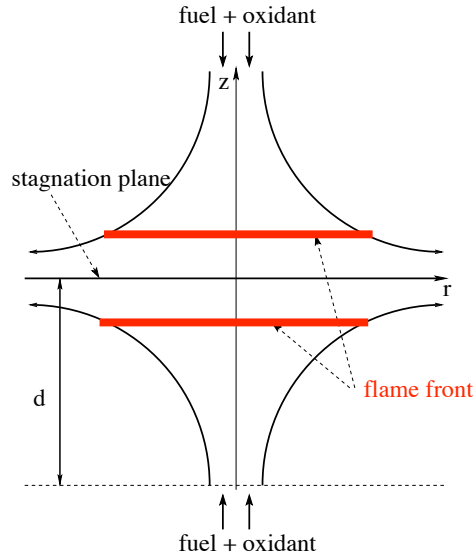


Figure 9: Schematic configuration of the counterflow, premixed flames.

References

- [1] A. Abdulle. Fourth order Chebyshev methods with recurrence relation. *SIAM J. Sci. Comput.*, 23(6):2041–2054 (electronic), 2002.
- [2] Y. D’Angelo and B. Larrouturou. Comparison and analysis of some numerical schemes for stiff complex chemistry problems. *RAIRO Modél. Math. Anal. Numér.*, 29(3):259–301, 1995.
- [3] N. Darabiha. Transient behaviour of laminar counterflow hydrogen-air diffusion flames with complex chemistry. *Comb. Sci. and Tech.*, 86:163–181, 1992.
- [4] P. de Mottoni and M. Schatzman. Geometrical evolution of developed interfaces. *Trans. Amer. Math. Soc.*, 347(5):1533–1589, 1995.
- [5] S. Descombes, M. Duarte, T. Dumont, V. Louvet, and M. Massot. Adaptive time splitting method for multi-scale evolutionary partial differential equations. *Confluentes Math.*, 3(3):413–443, 2011.
- [6] S. Descombes, T. Dumont, V. Louvet, and M. Massot. On the local and global errors of splitting approximations of reaction-diffusion equations with high spatial gradients. *Int. J. Comput. Math.*, 84(6):749–765, 2007.
- [7] S. Descombes and M. Massot. Operator splitting for nonlinear reaction-diffusion systems with an entropic structure: singular perturbation and order reduction. *Numer. Math.*, 97(4):667–698, 2004.

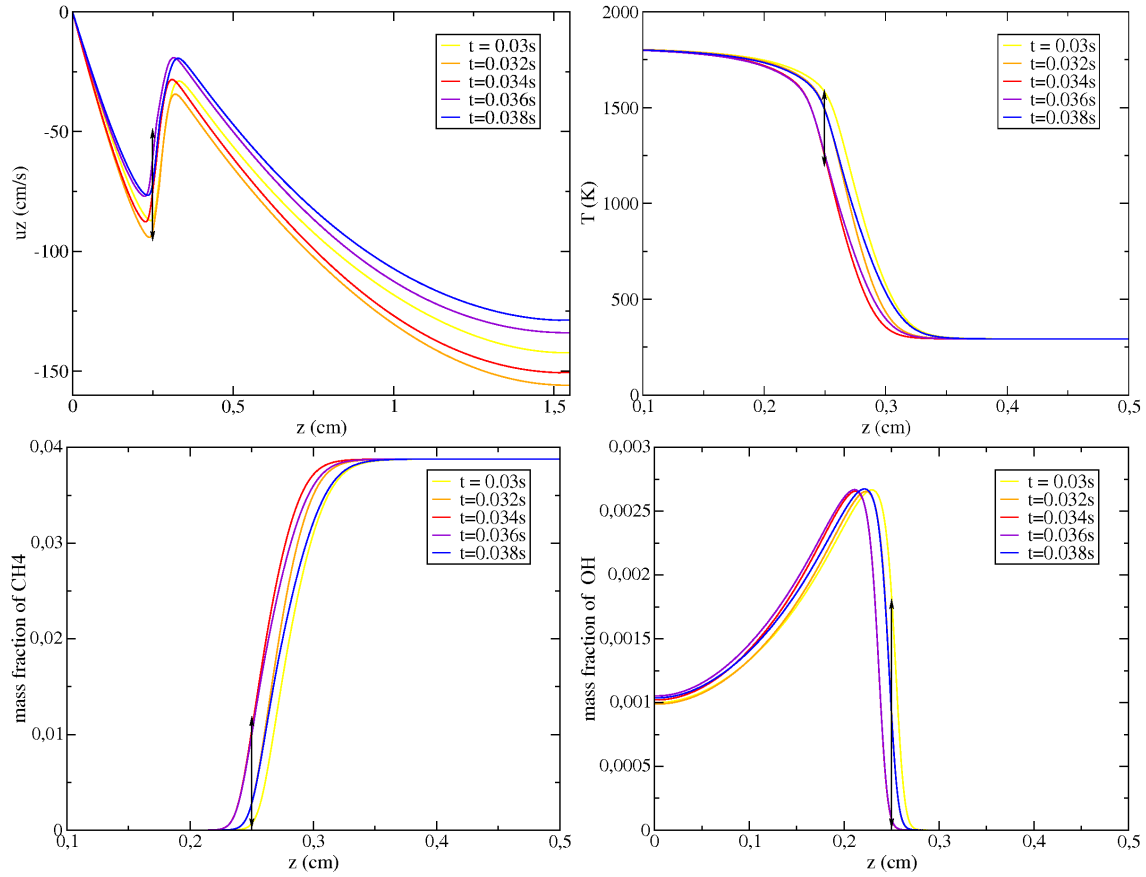


Figure 10: Top: time variations of axial velocity u_z (left) and temperature T (right) profiles. Bottom: mass fraction profiles for Y_{CH_4} (left) and Y_{OH} (right). Position $z = 0.25$ cm is indicated.

- [8] S. Descombes and M. Schatzman. Strang's formula for holomorphic semi-groups. *J. Math. Pures Appl.* (9), 81(1):93–114, 2002.
- [9] S. Descombes and M. Thalhammer. The Lie-Trotter splitting for nonlinear evolutionary problems with critical parameters: a compact local error representation and application to nonlinear Schrödinger equations in the semiclassical regime. *IMA J. Numer. Anal.*, 33(2):722–745, 2013.
- [10] M. Duarte, S. Descombes, C. Tenaud, S. Candel, and M. Massot. Time-space adaptive numerical methods for the simulation of combustion fronts. *Combust. Flame*, (160):1083–1101, 2013.
- [11] M. Duarte, M. Massot, and S. Descombes. Parareal operator splitting techniques for multi-scale reaction waves: numerical analysis and strategies. *ESAIM Math. Model. Numer. Anal.*, 45(5):825–852, 2011.
- [12] M. Duarte, M. Massot, S. Descombes, C. Tenaud, T. Dumont, V. Louvet, and F. Laurent. New resolution strategy for multi-scale reaction waves using time operator splitting, space adaptive multiresolution and dedicated high order implicit/explicit time integrators. *SIAM J. Sci. Comput.*, 34(1):A76–A104, 2012.

- [13] T. Dumont, M. Duarte, S. Descombes, M.-A. Dronne, M. Massot, and V. Louvet. Simulation of human ischemic stroke in realistic 3D geometry. *Commun. Nonlinear Sci. Numer. Simulat.*, 18(6):1539–1557, 2013.
- [14] A. Ern and V. Giovangigli. *Multicomponent transport algorithms*. Springer-Verlag, Berlin, 1994.
- [15] E. Faou, A. Ostermann, and K. Schratz. Analysis of exponential splitting methods for inhomogeneous parabolic equations. *To appear in IMA J. Numer. Anal.*, 2014.
- [16] L.P. Gao, Y. D’Angelo, I. Silverman, A. Gomez, and M.D. Smooke. Quantitative comparison of detailed numerical computations and experiments in counterflow spray diffusion flames. *Symp. (Int.) Comb.*, 26(1):1739–1746, 1996.
- [17] V. Giovangigli. *Multicomponent flow modeling*. Modeling and Simulation in Science, Engineering and Technology. Birkhäuser Boston Inc., Boston, MA, 1999.
- [18] P. Gray and S.K. Scott. *Chemical Oscillations and Instabilities*. Oxford Univ. Press, 1994.
- [19] E. Hairer, C. Lubich, and G. Wanner. *Geometric Numerical Integration*. Springer-Verlag, Berlin, 2nd edition, 2006. Structure-Preserving Algorithms for Ordinary Differential Equations.
- [20] E. Hairer and G. Wanner. *Solving Ordinary Differential Equations II*. Springer-Verlag, Berlin, 2nd edition, 1996. Stiff and Differential-Algebraic Problems.
- [21] E. Hansen, F. Kramer, and A. Ostermann. A second-order positivity preserving scheme for semilinear parabolic problems. *Appl. Numer. Math.*, 62(10):1428–1435, 2012.
- [22] E. Hansen and A. Ostermann. High order splitting methods for analytic semigroups exist. *BIT*, 49(3):527–542, 2009.
- [23] W. Hundsdorfer and J.G. Verwer. A note on splitting errors for advection-reaction equations. *Appl. Numer. Math.*, 18(1-3):191–199, 1995.
- [24] W. Hundsdorfer and J.G. Verwer. *Numerical Solution of Time-Dependent Advection-Diffusion-Reaction Equations*. Springer-Verlag, Berlin, 2003.
- [25] T. Ichinose and H. Tamura. The norm convergence of the Trotter-Kato product formula with error bound. *Comm. Math. Phys.*, 217(3):489–502, 2001.
- [26] T. Jahnke and C. Lubich. Error bounds for exponential operator splittings. *BIT*, 40(4):735–744, 2000.
- [27] A.N. Kolmogoroff, I.G. Petrovsky, and N.S. Piscounoff. Étude de l’équation de la diffusion avec croissance de la quantité de matière et son application à un problème biologique. *Bulletin de l’Université d’État Moscou*, 1:1–25, 1937.
- [28] R. Kozlov, A. Kværnø, and B. Owren. The behaviour of the local error in splitting methods applied to stiff problems. *J. Comput. Phys.*, 195(2):576–593, 2004.
- [29] F. Laurent, T. Schuller, C. Goepfert, N. Darabiha, J.C. Rolon, and M. Massot. Dynamical response of a premixed counter-flow flame: Numerical simulations and experimental measurements. In *Proc. Eleventh Int. Conf. Numer. Combust.*, 2006.
- [30] C. Lubich. On splitting methods for Schrödinger-Poisson and cubic nonlinear Schrödinger equations. *Math. Comp.*, 77(264):2141–2153, 2008.

- [31] A.J. Majda and J. Sethian. The derivation and numerical solution of the equations for zero Mach number combustion. *Comb. Sci. and Tech.*, 42:185–205, 1985.
- [32] G.I. Marchuk. Splitting and alternating direction methods. In *Handbook of numerical analysis, Vol. I*, Handb. Numer. Anal., I, pages 197–462. North-Holland, Amsterdam, 1990.
- [33] M. Massot, M. Kumar, M.D. Smooke, and A. Gomez. Spray counterflow diffusion flames of heptane: Experiments and computations with detailed kinetics and transport. *Symp. (Int.) Comb.*, 27(2):1975–1983, 1998.
- [34] D.L. Ropp and J.N. Shadid. Stability of operator splitting methods for systems with indefinite operators: reaction-diffusion systems. *J. Comput. Phys.*, 203(2):449–466, 2005.
- [35] D.L. Ropp, J.N. Shadid, and C.C. Ober. Studies of the accuracy of time integration methods for reaction-diffusion equations. *J. Comput. Phys.*, 194(2):544–574, 2004.
- [36] Q. Sheng. Global error estimates for exponential splitting. *IMA J. Numer. Anal.*, 14(1):27–56, 1994.
- [37] M.D. Smooke, J. Crump, K. Seshadri, and V. Giovangigli. Comparison between experimental measurements and numerical calculations of the structure of counterflow, diluted, methane-air, premixed flames. *Symp. (Int.) Comb.*, 23(1):463–470, 1991.
- [38] B. Sportisse. An analysis of operator splitting techniques in the stiff case. *J. Comput. Phys.*, 161(1):140–168, 2000.
- [39] B. Sportisse, G. Bencteux, and P. Plion. Method of lines versus operator splitting for reaction-diffusion systems with fast chemistry. *Environ. Model. Software*, 15(6-7):673–679, 2000.
- [40] G. Strang. On the construction and comparison of difference schemes. *SIAM J. Numer. Anal.*, 5:506–517, 1968.
- [41] R. Témam. Sur l’approximation de la solution des équations de Navier-Stokes par la méthode des pas fractionnaires. I. *Arch. Rational Mech. Anal.*, 32:135–153, 1969.
- [42] R. Témam. Sur l’approximation de la solution des équations de Navier-Stokes par la méthode des pas fractionnaires. II. *Arch. Rational Mech. Anal.*, 33:377–385, 1969.
- [43] J. G. Verwer, E. J. Spee, J. G. Blom, and W. Hundsdorfer. A second-order Rosenbrock method applied to photochemical dispersion problems. *SIAM J. Sci. Comput.*, 20(4):1456–1480, 1999.
- [44] N.N. Yanenko. *The method of fractional steps. The solution of problems of mathematical physics in several variables*. Springer-Verlag, New York, 1971.
- [45] B. Yang and S.B. Pope. An investigation of the accuracy of manifold methods and splitting schemes in the computational implementation of combustion chemistry. *Combust. Flame*, 112(1-2):16–32, 1998.